



UNIVERSITY OF LEEDS

This is a repository copy of *Modelling capillary oxygen supply capacity in mixed muscles: capillary domains revisited.*

White Rose Research Online URL for this paper:
<http://eprints.whiterose.ac.uk/88456/>

Version: Accepted Version

Article:

Al-Shammari, AA, Gaffney, EA and Egginton, S (2014) Modelling capillary oxygen supply capacity in mixed muscles: capillary domains revisited. *Journal of Theoretical Biology*, 356. 47 - 61. ISSN 0022-5193

<https://doi.org/10.1016/j.jtbi.2014.04.016>

© 2014. This manuscript version is made available under the CC-BY-NC-ND 4.0 license
<http://creativecommons.org/licenses/by-nc-nd/4.0/> ↗

Reuse

Unless indicated otherwise, fulltext items are protected by copyright with all rights reserved. The copyright exception in section 29 of the Copyright, Designs and Patents Act 1988 allows the making of a single copy solely for the purpose of non-commercial research or private study within the limits of fair dealing. The publisher or other rights-holder may allow further reproduction and re-use of this version - refer to the White Rose Research Online record for this item. Where records identify the publisher as the copyright holder, users can verify any specific terms of use on the publisher's website.

Takedown

If you consider content in White Rose Research Online to be in breach of UK law, please notify us by emailing eprints@whiterose.ac.uk including the URL of the record and the reason for the withdrawal request.



eprints@whiterose.ac.uk
<https://eprints.whiterose.ac.uk/>

Modelling **capillary oxygen supply** capacity in mixed muscles: Capillary domains revisited

Abdullah A. Al-Shammari^{1,2*}, Eamonn A. Gaffney¹, Stuart Egginton³

¹Wolfson Centre for Mathematical Biology, Mathematical Institute, University of Oxford, Woodstock Road, Oxford OX2 6GG, United Kingdom.

²Department of Mathematics, Faculty of Sciences, Kuwait University, P.O. Box 5969, Khaldiya 13060, Kuwait.

³School of Biomedical Sciences, Faculty of Biological Sciences, University of Leeds, Leeds LS2 9JT, United Kingdom.

*Author for Correspondence. *Tel.*: +44 1865 283878; *E-mail Address*: alshammari@maths.ox.ac.uk

Abstract

Developing effective therapeutic interventions for pathological conditions associated with abnormal oxygen transport to muscle fibres critically depends on the objective characterisation of capillarity. Local indices of capillary supply have the potential to identify the onset of fine-scale tissue pathologies and dysregulation. Detailed tissue geometry, such as muscle fibre size, has been incorporated into such measures by considering the distribution of Voronoi polygons (VP) generated from planar capillary locations as a representation of capillary supply regions. Previously, detailed simulations have predicted **that** this is generally accurate for muscle tissue with uniform oxygen uptake. Here we extend this modelling framework to heterogeneous muscle for the assessment of *capillary supply capacity* under maximal sustainable oxygen consumption. We demonstrate for muscle with heterogeneous fibre properties that VP theoretically provide a computationally simple but often accurate representation of trapping regions (TR), which are predicted from biophysical transport models to represent the areas of tissue supplied **by** individual capillaries. However, this use of VP may become less accurate around large fibres, and at the interface of fibres of largely different oxidative capacities. In such cases, TR may provide a more robust representation of capillary supply regions. Additionally, given VP can only approximate oxygen delivery by capillaries, we show that their **generally close relationship** to TR suggests that (1) fibre type distribution may be tightly regulated to avoid large fibres with high oxidative capacities, (2) the anatomical fibre distribution is also tightly regulated to prevent large surface area of interaction between metabolically dissimilar fibres, and (3) in chronically hypoxic tissues capillary distribution is more important in determining oxygen supply than the spatial heterogeneity of fibre demand.

Keywords Mathematical modelling, Capillary supply regions, Capillary domains, Fibre type, Skeletal muscle

1 Introduction

The objective assessment of anatomical capillary supply to striated muscle fibres is contingent on using methods that can accurately capture tissue capillarity while also unambiguously linking the local capillary distribution to the global supply. A survey of the recent literature on the quantitative assessment of **capillary supply in striated muscle** identifies two general morphometric methods for analysing tissue capillarisation in an effort to assess functional consequences (Hoofd et al., 1985; Hudlická et al., 1992; Degens et al., 1992; Egginton & Ross, 1992; Egginton, 2002; Ahmed et al., 1997; Suzuki et al., 2000; Wüst et al., 2009a,b, 2012). First, global methods use average values of structural composition or functional activity to represent the tissue uniformly, e.g. mean intercapillary distance (ICD), mean capillary density (CD), mean capillary-to-fibre ratio (C:F), and mean oxygen uptake (MO_2). However, average indices cannot capture the spatial heterogeneity in capillary supply generated by the local metabolic environment and the distribution of fibre size (Ahmed et al., 1997), and the scale-dependency inherent in such indices may explain why data on capillarity is variable, if not conflicting (Egginton, 1990). Second, area-based methods, such as those based on Krogh cylinders (Krogh, 1919) or Voronoi polygons (equivalently known as capillary domains; Hoofd et al., 1985), are used to avoid the spatial limitations of models based on global indices. A capillary domain is defined to be the area of a muscle cross section surrounding an individual capillary and closer to its centre than all neighbouring capillaries. The resulting polygonal tessellation potentially captures the local environment of capillaries, with each 2-dimensional domain contained in the cross section approximating the supply region of the capillary it encloses.

Krogh cylinders, however, are inadequate for this role since they lead to nonphysiological tissue voids and overlaps. In contrast, Voronoi polygons (Fig. 1B) generate a space-filling alternative (Egginton & Ross, 1989, 1992) thereby allowing the exploration of the local influences associated with microvascular remodelling, as well as any mismatch between angiogenesis and local O_2 demand (Degens et al., 1992, 2002, 2006, 2008; Egginton et al., 2001; Wüst et al., 2009a). This gives Voronoi polygons an advantage in assessing the efficacy of applications to pathological scenarios, such as ischaemia, where potential therapeutic interventions include strength training (Deveci & Egginton, 2002; Suzuki et al., 2000), endurance exercise (Ahmed et al., 1997; Scott et al., 2009), electrical stimulation (Ebina et al., 2002), and alterations in muscle temperature (Egginton et al., 2001; Egginton, 2002). In addition to their ability to reproduce robust versions of the aforementioned global measures, Voronoi polygons have the capacity to provide indices of capillary supply to individual fibres, with both direct contact and indirect influence, and to fibres of different metabolic activities. For instance, the local capillary-to-fibre ratio (LCFR) and the local capillary density around fibres (LCD; also known as the capillary fibre density, CFD) are obtained from the cumulative overlap of Voronoi polygons with individual muscle fibres (Egginton & Ross, 1989). These indices have continuous distributions that are based on both adjacent and remote capillaries, thus allowing for the experimental observation of fibres that are supplied by capillaries with no direct contact (Egginton, 1990; Wüst et al., 2009a).

Although experimental studies of muscle tissue capillarity that are based on Voronoi polygons have revealed intricate details about the regulatory process of microvascular remodelling, there is yet to be a 3-dimensional theoretical exploration of capillary supply regions and their correlation with Voronoi polygons (Goldman, 2008). In contrast, such correlations have been explored in two dimensions only (e.g. Hoofd et al., 1990; Wang & Bassingthwaight,

2001; Egginton & Gaffney, 2010; Al-Shammari et al., 2012). In particular, for moderately symmetric capillary distributions within tissues of homogeneous oxygen uptake, Hoofd and colleagues (1990) were able to qualitatively show the majority of oxygen fluxes from capillaries are captured within the corresponding Voronoi polygons. Nonetheless, some results indicated that more heterogeneous capillary arrangements may reduce this correlation, in agreement with a recent geometrical demonstration (Egginton & Gaffney, 2010), thus highlighting that further investigation in this direction is needed.

Wang & Bassingthwaite (2001) explored this question and criticised the use of Voronoi polygons for asymmetrical capillary arrangements, concluding that they are inappropriate. However, in order to make the mathematical analysis more tractable, they considered unphysiologically low capillary densities (maximum of 7 capillaries per tissue cross section) which, in turn, exposed predictions of capillary supply regions to boundary artefacts. In contrast, we have recently addressed these complications *via* exploring a much larger number of capillary supply areas within a sub-region of **homogeneous** muscle tissue cross sections where boundary artefacts are negligible (Al-Shammari et al., 2012). In particular, noting that *trapping regions* denote the prediction of capillary supply regions from biophysical models of oxygen transport and kinetics, we demonstrated that Voronoi polygons generally give an accurate approximation of trapping regions within muscle tissues consuming oxygen uniformly at maximal capacity. Nonetheless, we also observed that the approximation accuracy may deteriorate with rising levels of capillary rarefaction, and may ultimately break down under significant perturbations to the uniformity of muscle oxygen tension (PO_2). However, such complications under maximal functional supply require tissue pathology and hence we predicted that correlations between Voronoi polygons and supply regions may reflect local control of angiogenic foci on the length-scale of a muscle fibre diameter, thus preventing random capillary rarefaction as observed by Badr et al. (2003).

In contrast to the homogeneity in oxidative metabolism typically found in cardiac muscle tissue, skeletal muscle fibres often exhibit heterogeneous functional as well as structural characteristics. The transport properties associated with fibre microstructure and composition (e.g. myoglobin content and lipid stores), the metabolic demand for oxygen, and the fibre size in animals are dependent on fibre type (Jürgens et al., 1994; Meng et al., 1993; Hoofd & Egginton, 1997; Wüst et al., 2009a; Egginton, 1990). Additionally, capillary arrangements in skeletal muscle tissues have been observed to be regulated by fibre type and size (**Ahmed et al., 1997; Wüst et al., 2009b**). **In particular, the heterogeneity of capillary spacing may be partly determined by the heterogeneity in fibre size (Egginton et al., 1988; Egginton & Ross, 1989)**. Furthermore, the influence of fibre heterogeneities has been explored in numerical simulations by Liu et al. (2012), who concluded that changes in the fibre size distribution and oxygen uptake associated with different fibre types were particularly influential in the context of PO_2 heterogeneity within mixed muscles. Nevertheless, it is unknown whether a strong correlation between Voronoi polygons and capillary supply areas should hold in the presence of such heterogeneities. Hence, it is unclear whether measures based on Voronoi polygons are appropriate in other physiological settings such as tissue hypoxia given heterogeneous fibre-dependent properties (e.g. metabolic activity, geometry, oxygen diffusivity, and myoglobin content and facilitation). Therefore, our objective is to extend our previous model of oxygen transport under maximal sustainable conditions in tissue, characterising when and where indices based on Voronoi polygons are likely to accurately assess O_2 supply from capillary distributions embedded in functionally heterogeneous tissue, e.g. skeletal muscle. As Voronoi polygons are generated with relative computational ease and require no parameter estimation,

we additionally seek to assess their accuracy in terms of the less accessible trapping regions approach. In line with the direction of our recent publication (Al-Shammari et al., 2012), we also investigate correlations between Voronoi polygons and trapping regions in an effort to characterise capillary supply in different physiological scenarios and to highlight possible regulatory mechanisms in skeletal muscles.

2 Theory

The cross section in Fig. 1A is a light microscopy image of rat hindlimb skeletal muscle, *m. extensor digitorum longus*, prepared *via* flash freezing in liquid nitrogen-cooled isopentane and cryostat sectioned at $-20\text{ }^\circ\text{C}$ with the capillary location identified using alkaline phosphatase staining (Egginton et al., 2001).

We consider such a tissue cross section, where capillary locations are represented by a single point, e.g. the centroid of each capillary in the image plane of the muscle cross section. Given these cross sections we first of all want to estimate the *capillary supply domains*, that is the region of tissue supplied by each capillary and two theoretical predictions for these domains, in the form of Voronoi Polygons and Trapping Regions. These are mathematically defined below, together with derivative measures. In particular, Voronoi polygons are simple to determine and based on geometry only, whereas trapping regions are ultimately found by solving the equations associated with the biophysical oxygen transport problem. Our objective therefore reduces to assessing whether the underlying biophysics, in the form of trapping regions predictions for the capillary supply domains, supports the use of simpler Voronoi polygons approximations, together with associated derivative indices, for characterising capillary supply domains under maximal sustainable conditions.

2.1 Voronoi polygons

Let N_c denote the number of capillaries, and \mathbf{x}_i denote the position of the **centroid of the** i^{th} capillary with Ω representing the global domain. The Voronoi polygon (VP), also referred to as the capillary domain, that is associated with the i^{th} capillary is a 2-dimensional region surrounding it with boundaries that are equidistant from adjacent capillaries (Fig. 1B). Thus, the VP containing the i^{th} capillary with centre \mathbf{x}_i is the set

$$V_i = \left\{ \mathbf{x} \mid \mathbf{x} \in \Omega; \|\mathbf{x} - \mathbf{x}_i\| \leq \|\mathbf{x} - \mathbf{x}_k\|, k \neq i \right\}, \quad (1)$$

with ∂V_i **denoting the boundary of** V_i **and** the collection of VP associated with all capillaries tessellating the entire domain, Ω ,

$$\Omega = \bigcup_{i=1}^{N_c} V_i,$$

$$V_i \cap V_j = \partial V_i \cap \partial V_j, i \neq j.$$

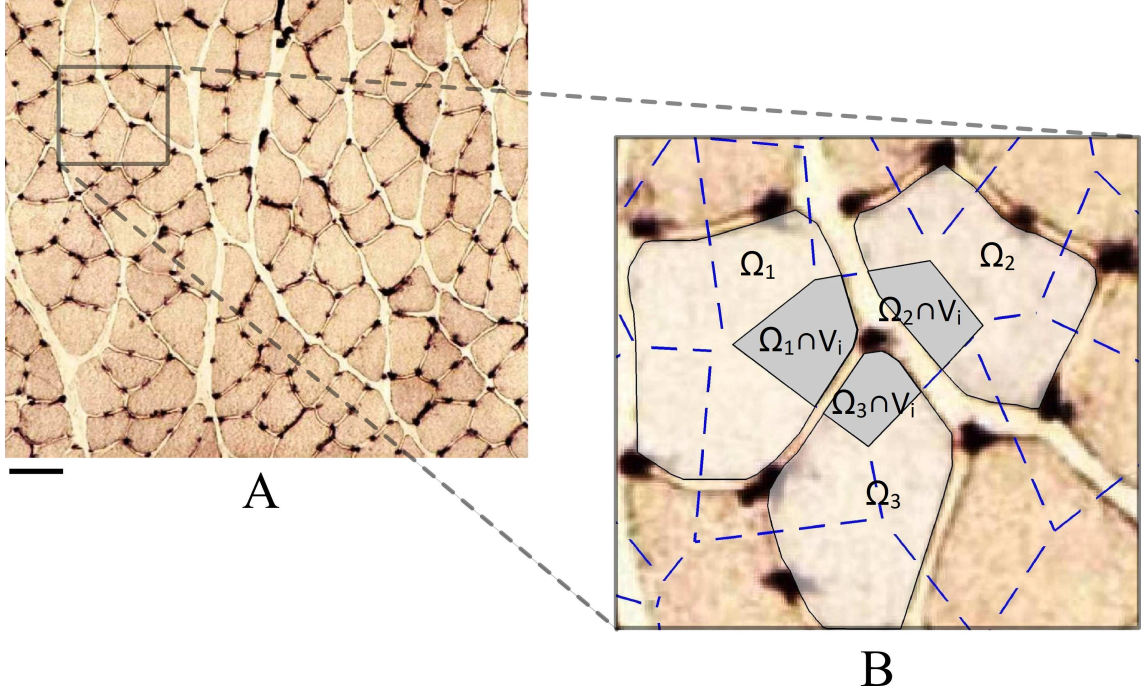


Figure 1: (A) Typical tissue cross section of rat skeletal muscle (*m. extensor digitorum longus*) with capillary location identified by alkaline phosphatase staining. The dark structures are capillaries, the lighter objects are muscle fibres, and the lightest region is the interstitial space. Note the heterogeneity of intercapillary distances between adjacent vessels, in part reflecting heterogeneity of cell size in the host tissue (Egginton et al., 1988; Egginton & Ross, 1989). The scale bar corresponds to 50 μm . (B) An expanded region of the original image on which a Voronoi tessellation is superimposed by dotted blue lines. A central Voronoi polygon, V_i , is highlighted in *dark gray* and overlaps adjacent fibres denoted by Ω_1 , Ω_2 , and Ω_3 (*light gray*) with the overlapping regions $\Omega_1 \cap V_i$, $\Omega_2 \cap V_i$, and $\Omega_3 \cap V_i$ representing the fractional supply area of this Voronoi polygon to each fibre. The symbol \cap denotes the intersection of or overlap between two regions. (Online version in colour).

Derivative indices of the functional capillary supply for maximal muscle capacity are the local capillary-to-fibre ratio (LCFR) and the local capillary density (LCD; also known as the capillary fibre density, CFD). To define these, we let Ω_j denote the region of the j^{th} fibre and $A(\cdot)$ denote the 2-dimensional Euclidean area measure. Then the LCFR and LCD of the j^{th} muscle fibre are defined with respect to VP as

$$LCFR_j^{VP} = \sum_i \frac{A(\Omega_j \cap V_i)}{A(V_i)}, \quad LCD_j^{VP} = \frac{1}{A(\Omega_j)} \sum_i \frac{A(\Omega_j \cap V_i)}{A(V_i)}, \quad (2)$$

respectively. Here, $LCFR_j^{VP}$ denotes the sum of the fractions of each VP area overlapping the j^{th} fibre (Fig. 1B). This index represents the fractional number of capillaries supplying the j^{th} muscle fibre with oxygen, i.e. the number of capillary equivalents of supply at maximum capacity. Similarly, LCD_j^{VP} is the number of capillaries supplying the j^{th} muscle fibre per unit fibre area.

2.2 Trapping regions

For a given capillary with a positive oxygen flux at its boundary, the *trapping region* (TR) is the smallest domain enclosing the capillary with zero flux conditions on its boundary. Thus, given a solution of the model equations for tissue oxygen partial pressure p , the trapping region $D_i \subseteq \Omega$ of a capillary with centre \mathbf{x}_i , with outward pointing normal \mathbf{n}_i , is defined to be the smallest domain within a closed boundary containing \mathbf{x}_i and satisfying

$$D_i = \left\{ \mathbf{x} \in \Omega \mid \mathbf{n}_i \cdot \nabla p = 0, \mathbf{x} \in \partial D_i \right\}. \quad (3)$$

Clearly, the above is a model-dependent definition. Each D_i yields the area surrounding a capillary where the outward flux due to the i^{th} capillary is balanced by **the inward flux due to all** neighbouring capillaries of contiguous supply regions. In addition, the regions D_i need not tessellate Ω ; if they do not, then there is at least one region in Ω which does not receive any oxygen from any capillary, which is a mathematical possibility but not a reasonable physiological one. Moreover, the analogous derivative indices, local capillary-to-fibre ratio ($LCFR_j^{TR}$) and local capillary density (LCD_j^{TR}), are similar to those derived for Voronoi polygons with D_i replacing V_i

$$LCFR_j^{TR} = \sum_i \frac{A(\Omega_j \cap D_i)}{A(D_i)}, \quad LCD_j^{TR} = \frac{1}{A(\Omega_j)} \sum_i \frac{A(\Omega_j \cap D_i)}{A(D_i)}. \quad (4)$$

By construction, and under maximal sustainable oxygen consumption, D_i represents the region of supply of each capillary according to the model used to determine tissue oxygen partial pressure p . When a VP is used to represent the region of capillary supply, the validity of this assumption dictates the validity of the above capillary supply capacity indices. Thus, we are interested in delimiting when the i^{th} Voronoi polygon, V_i , yields a good approximation to the i^{th} trapping region, D_i .

3 Methods

An extension of a previously published oxygen transport model under maximal sustainable conditions (Al-Shammari et al., 2012) is developed to explore the validity of Voronoi polygons for use in morphometric analyses of mixed muscle tissues with heterogeneous metabolic activities and anatomical properties, as found in mixed muscles. Thus we consider muscle tissues with either uniform or non-uniform functional characteristics, which allows an exploration general enough to cover both skeletal and cardiac muscles. A typical muscle is exemplified by the tissue cross section presented in Fig. 1, where the lengthscale of a capillary cross-section is taken to be 2-4 μm . In addition, we also incorporate facilitated diffusion and Michaelis-Menten kinetics of O_2 consumption into the transport equation to account for myoglobin-facilitated diffusion and **to** explore the consequences of tissue hypoxia.

3.1 Model formulation

Oxygen transport is explored in a two-dimensional domain representing a cross section of a skeletal or cardiac muscle tissue. In the section transversal to this domain, an array of capillaries of small circular cross-sectional shape supply the tissue with oxygen through passive diffusion. **Since the ratio of the characteristic intercapillary distance to capillary length is sufficiently small ($\mathcal{O}(10^{-2})$), tissue diffusion along the direction of the fibre axis can be neglected under maximal sustainable conditions and away from the arteriolar and venous ends of capillaries (Fletcher, 1980; Gayeski & Honig, 1988; Whiteley et al., 2002).**

3.1.1 Equations

An extension of our recent model of oxygen steady-state diffusion in tissue is used to explore further the diffusive analogue of Voronoi polygons under conditions of compartment-specific diffusion and uptake, myoglobin-facilitated diffusion, and oxygen consumption rate with Michaelis-Menten kinetics.

We exploit a single partial differential equation describing oxygen diffusion in muscle tissue fibres and interstitial spaces *via* incorporating compartment-specific biophysical parameters, thus allowing for the consequential differences in O_2 diffusion resulting from the local heterogeneity in oxidative metabolism to be explored. In addition, intravascular transport is averaged out and incorporated *via* a boundary condition at capillary walls. For the purpose of exploring the appropriateness of Voronoi polygons, neglecting intravascular heterogeneities is appropriate as the primary assumption is that the tissue is under maximal sustainable (aerobic) activity.

Consequently, oxygen transport in each tissue compartment β is described by the local free oxygen partial pressure (PO_2), denoted by p , which is governed by

$$\nabla \cdot \left[D_\beta \nabla(a_\beta p) + C_\beta^{Mb} D_\beta^{Mb} \left(\frac{dS_{Mb}}{dp} \nabla p \right) \right] - M_\beta(p) = 0, \quad (5)$$

where D_β and a_β are the molecular diffusivity and solubility of free oxygen, C_β^{Mb} and D_β^{Mb} are the bulk myoglobin (Mb) concentration and diffusivity, and M_β is the rate of O_2 consumption in muscle tissue compartment β . Here β denotes the following tissue compartments: *interstitial spaces* ($\beta = IS$) and *fibre types I* ($\beta = I$), *IIa* ($\beta = IIa$), and *IIb* ($\beta = IIb$). **Note that a_β is constant below and thus $\nabla(a_\beta p) = a_\beta \nabla p$.**

Assuming a homogeneous distribution of myoglobin molecules within muscle fibres and rapid local kinetics of Mb- O_2 dissociation, the equilibrium O_2 -saturation of Mb is governed by

$$S_{Mb}(p) = \frac{p}{p + p_{50,Mb}}, \quad (6)$$

where $p_{50,Mb}$ is the tissue oxygen partial pressure at half Mb-saturation.

Within muscle fibres, the rate of oxygen consumption by a tissue compartment is assumed to follow Michaelis-Menten kinetics described by

$$M_\beta(p) = \frac{M_0^\beta p}{p + p_c}, \quad (7)$$

where M_0^β is the maximal consumption rate volume-averaged over tissue compartment β , and p_c is the tissue PO_2 value which reflects the partial pressure scale where fibre mitochondria are no longer able to extract oxygen at maximal rate. We note that due to the near absence of myoglobin binding and consumption of free oxygen in interstitial spaces, the steady-state equation governing oxygen transport in this compartment is reduced to

$$a_{IS} D_{IS} \nabla^2 p = 0. \quad (8)$$

The domain geometry is obtained by considering a circular tissue cross section and then rescaling to the unit disk, \mathbb{D}^1 . After rescaling, the region enclosed by compartment β will be denoted by Ω_β with boundary $\partial\Omega_\beta$. Capillaries are assumed to possess an area, C_i , with a boundary, ∂C_i , though below we treat the capillaries as small circles with radius r_{cap} . Therefore, we seek to investigate PO_2 in a region of the unit disk that excludes the capillary lumina, $\Omega = \bigcup_\beta \Omega_\beta = \mathbb{D}^1 \setminus \bigcup_i C_i$.

3.1.2 Boundary conditions

The exchange of oxygen between capillaries and the interstitial fluid or fibres occur at their respective interfaces. Across the part of the capillary wall in contact with either the interstitial fluid or fibres, passive permeation of oxygen into tissue is characterised by the boundary condition for the i^{th} capillary

$$\mathbf{n}_i \cdot (a_\beta D_\beta \nabla p) = k(p_{\text{cap}} - p), \quad \partial C_i \cap \partial\Omega_\beta, \quad (9)$$

where \mathbf{n}_i is the unit normal vector on the capillary wall pointing away from the tissue and into the capillary, k is the mass transfer coefficient, p_{cap} is the transversally-averaged intracapillary PO_2 , and p is the partial pressure of oxygen at the external capillary wall. At the interstitium-fibre and fibre-fibre interfaces we assume continuity of oxygen flux and concentration

$$\mathbf{n}_\beta \cdot (a_\beta D_\beta \nabla p) = \mathbf{n}_\gamma \cdot (a_\gamma D_\gamma \nabla p), \quad \partial\Omega_\beta \cap \partial\Omega_\gamma, \quad (10)$$

$$a_\beta p = a_\gamma p, \quad \partial\Omega_\beta \cap \partial\Omega_\gamma. \quad (11)$$

Additionally, a no-flux boundary condition is imposed at the outer boundary of the tissue, effectively the muscle fascicle, to signify no exchange across it

$$\mathbf{n}_\beta \cdot \left(a_\beta D_\beta \nabla p \right) \Big|_{\partial\Omega} = 0. \quad (12)$$

As detailed elsewhere (Al-Shammari et al., 2012), perturbing the latter boundary condition is verified to induce no significant influence on the system behaviour away from the tissue domain boundary, thus justifying its use.

3.2 Non-dimensionalisation

To reduce the number of parameters, we non-dimensionalise the model as follows. Given that N_c capillaries in a tissue disk have an average capillary density ρ , the lengthscale, L , is taken to be equal to the diameter of the disk, which is given by $L = \sqrt{4N_c/\pi\rho}$. We use this along with p_{cap} , a_I , D_I , and M_0^I to non-dimensionalise our model by setting

$$\begin{aligned} x &= L\bar{x}, & p &= p_{cap}\bar{p}, & p_c &= p_{cap}\bar{p}_c, & p_{50,Mb} &= p_{cap}\bar{p}_{50,Mb}, & a_\beta &= a_I\bar{a}_\beta, \\ D_\beta &= D_I\bar{D}_\beta, & C_\beta^{Mb} &= C_I^{Mb}\bar{C}_\beta^{Mb}, & D_\beta^{Mb} &= D_I^{Mb}\bar{D}_\beta^{Mb}, & M_0^\beta &= M_0^I\bar{M}_0^\beta, \\ \theta_I &= \frac{C_I^{Mb}D_I^{Mb}}{a_I D_I p_{cap}}, & \mu_I &= \frac{L^2 M_0^I}{a_I D_I p_{cap}}, & \kappa_I &= \frac{Lk}{a_I D_I}, \end{aligned}$$

where the bars denote non-dimensional variables and parameters. Here $\theta_I, \mu_I, \kappa_I > 0$ are the non-dimensionalised myoglobin content, metabolic oxygen demand, and mass transfer coefficient of fibre type I. Dropping the bars, the non-dimensional model is given by

$$\nabla \cdot \left[\left(a_\beta D_\beta + C_\beta^{Mb} D_\beta^{Mb} \theta_I \frac{dS_{Mb}}{dp} \right) \nabla p \right] - M_0^\beta M_I(p) = 0, \quad x \in \Omega_\beta, \quad (13a)$$

$$n_i \cdot (a_\beta D_\beta \nabla p) = \kappa_I (1 - p), \quad x \in \partial C_i \cap \partial\Omega_\beta, \quad (13b)$$

$$n_\beta \cdot (a_\beta D_\beta \nabla p) = n_\gamma \cdot (a_\gamma D_\gamma \nabla p), \quad x \in \partial\Omega_\beta \cap \partial\Omega_\gamma, \quad (13c)$$

$$a_\beta p = a_\gamma p, \quad x \in \partial\Omega_\beta \cap \partial\Omega_\gamma, \quad (13d)$$

$$n_\beta \cdot \left(a_\beta D_\beta \nabla p \right) \Big|_{\partial\Omega} = 0, \quad (13e)$$

$$M_I(p) = \frac{\mu_I p}{p + p_c}, \quad S(p) = \frac{p}{p + p_{50,Mb}}. \quad (13f)$$

3.3 Domain geometry & functional characteristics

3.3.1 Fibre and capillary geometric distributions

We use three domain geometries that are characterised by fibre size and shape. The first geometry considered is synthetic uniform size distribution, SU, based on a total of 199 synthetic fibres

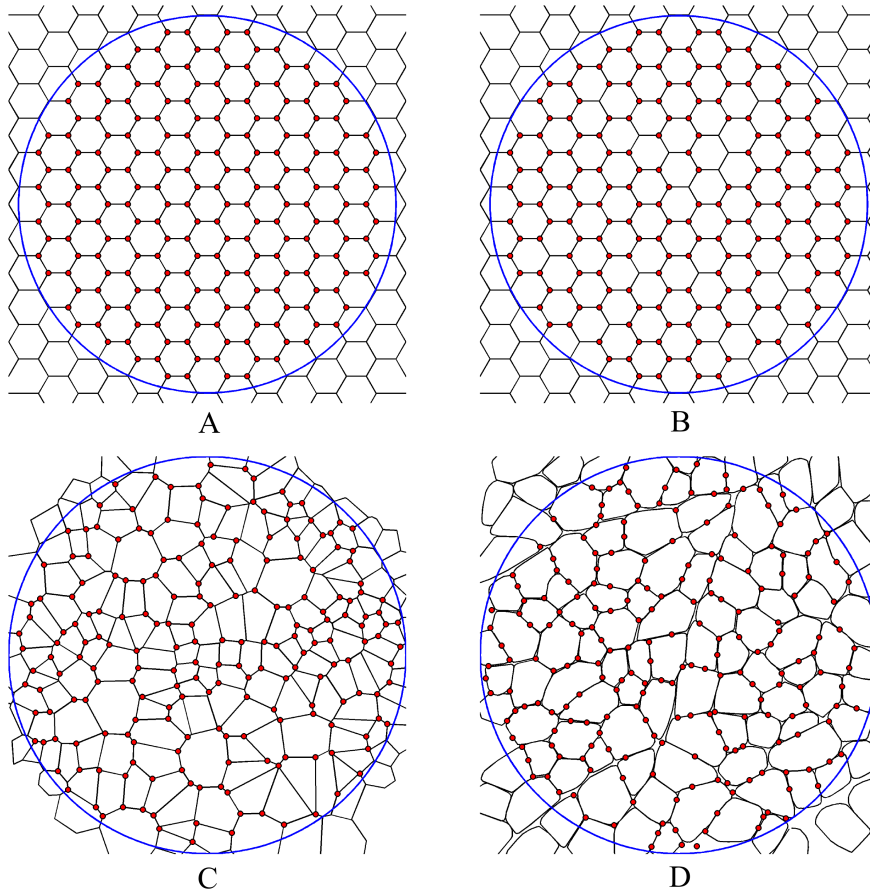


Figure 2: A view of modelling geometries. (A) Synthetic fibres of hexagonal shape and uniform size (SU) with capillaries placed on their vertices (symmetric capillary distribution). (B) The same fibre geometry as in (A) with 10% random capillary rarefaction irrespective of fibre type (SU_R). (C) Synthetic fibres of polygonal shape and non-uniform size with capillaries placed on fibre vertices (SN). Note that the fibre size non-uniformity reflects localised rarefactions around relatively large fibres. (D) A rat EDL muscle geometry (H). Traces of fibre cross sections and capillary centroid locations were made from slides using a microscope drawing arm and their x, y coordinates were registered on a digitising tablet.

of hexagonal shape and uniform size with capillaries placed at fibre vertices (Fig. 2A). These fibres are generated from a Voronoi tessellation of the plane based on hexagonal array of nodes with prescribed side length and the number of capillaries is determined by the lengthscale, L , and capillary density, ρ , which are extracted from histological data and illustrated in Fig. 2. For the final domain illustrated in Fig. 2A, 151 fibres are enclosed within a disk constituting the simulation domain, which is obtained by rescaling to the unit disk. We also consider a random local capillary rarefaction of SU, whereby 10% of the capillaries (about 21 in number) are removed at random, and denote the resulting geometry by SU_R (Fig. 2B). It should be noted here that no interstitial spaces are included in either of these geometries.

The second geometry, synthetic non-uniform size distribution (SN), is based on a total of 199 polygonal fibres of non-uniform size with capillaries placed at fibre vertices (Fig. 2C). These are generated from a Voronoi tessellation using nodes that have been placed on a random perturbation of the aforementioned hexagonal array. The final domain geometry encloses 183 fibres of different sizes and shapes and, once more, no interstitial spaces are included in this

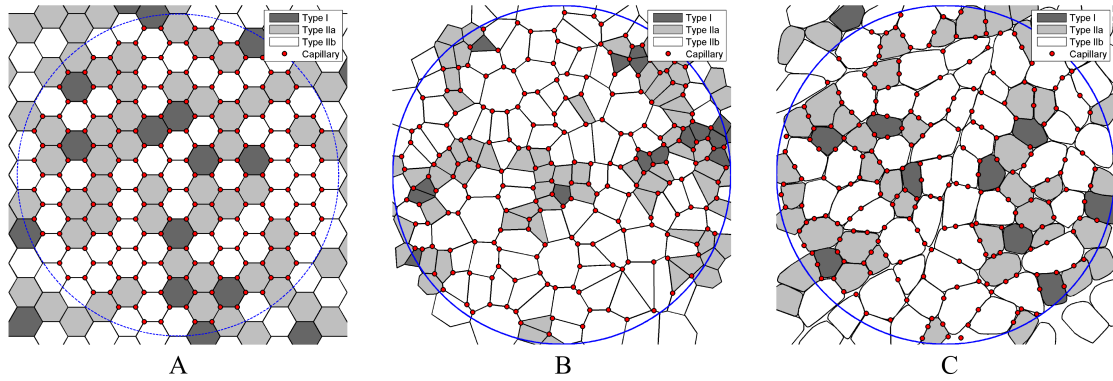


Figure 3: Examples of the fibre type distributions we use in our model. (A) A random distribution of a 9:37:54 (I:IIa:IIb) fibre-type composition. (B) A size-based distribution of 9:37:54 fibre type composition. (C) Fibre size and type distributions and fibre type composition (9:37:54) are obtained from histological sections of a rat EDL muscle with capillary locations identified *via* alkaline phosphatase staining and fibre types *via* succinate dehydrogenase and myosin ATPase staining.

geometry.

The third geometry is based on histological fibre size and type distribution (H), using a total of 114 fibres extracted from a digitized image of a rat EDL (*m. extensor digitorum longus*) muscle cross section (Fig. 2D). In this case, the final domain geometry is a disk enclosing 102 fibres and interstitial spaces.

3.3.2 Fibre type distribution & areal composition

The fibre type distribution in space is divided into three categories: random, size-based, and real. These are used selectively for the aforementioned geometries (Table I). In the case of a *random* distribution of fibre types, types I, IIa, and IIb are randomly assigned to fibres regardless of the underlying size distribution (e.g. Fig. 3A). Such random assignment is constrained by a predefined areal composition of fibre types (I:IIa:IIb). However, in our simulations, we often restrict ourselves to using only two fibre types (e.g. I & IIb) in order to have a control over potential fibre-fibre effects on supply regions. In the *size-based* case, the spatial assignment of fibre types is based on (1) their increasing size in the following order $I < IIa < IIb$ to reflect histological observations, and (2) a predefined areal composition (e.g. 50:0:50 and 9:37:54 as illustrated in 3B). We note here that, for the SU geometry, the uniformity in fibre sizes dictates a spatial randomness for all fibre-type assignments. Finally in Fig. 3C, we illustrate the *real* case where fibres are assigned the areal composition of a rat EDL muscle (9:37:54) with fibre-size

	Fibre type distribution						
	Random			Size-based		Real	
Areal Composition	0:0:100	25:0:75	50:0:50	75:0:25	100:0:0	50:0:50	9:37:54
Geometry	SU, SN	SU, SN	SU, SN, SU _R	SU, SN	SU, SN	SN	SU, SN, H

Table I: The spatial distribution (random, size-based, real) and areal composition (Type I:IIa:IIb) of fibre types, for domain geometries: SU = synthetic uniform size, SU_R = rarefied SU, SN = synthetic non-uniform size, and H = histologic size.

Parameter	Symbol	Fibre type, β			Units	Refs.
		I	IIa	IIb		
O ₂ demand	M_0^β	15.7	13.82	7.85	10 ⁻⁵ ml O ₂ /ml-s	Sullivan & Pittman (1984), Wüst et al. (2009b)
Mb concentration	C_β^{Mb}	10.2	4.98	1.55	10 ⁻³ ml O ₂ /ml	Meng et al. (1993)
O ₂ solubility	a_β		3.89×10^{-5}		ml O ₂ /ml-mmHg	Mahler et al. (1985), Christoforides et al. (1969)
O ₂ diffusivity	D_β		2.41×10^{-5}		cm ² /s	Bentley et al. (1993), Ellsworth & Pittman (1984)
Mb diffusivity	D_β^{Mb}		1.73×10^{-7}		cm ² /s	Jürgens et al. (1994)
Mass transfer coefficient	k		4.0×10^{-6}		ml O ₂ /cm ² -mmHg-s	Eggleton et al. (1998), Goldman & Popel (2000)
Intracapillary PO ₂	P_{cap}		20		mmHg	Eggleton et al. (2000)
Mb half-saturation PO ₂	$P_{50,Mb}$		5.3		mmHg	Jürgens et al. (1994)
PO ₂ at half demand	P_c		0.5		mmHg	Honig & Gayeski (1982)
Capillary radius	r		$1.8 - 2.5 \times 10^{-4}$		cm	Ellsworth et al. (1988)
Capillary density	ρ		913.4		mm ⁻²	*
# of capillaries	N_{cap}		204 - 215		unitless	*
Lengthscale	L		$5.33 - 5.47 \times 10^{-2}$		cm	
Transfer coefficient	κ_β		233.4		unitless	
O ₂ demand	μ_β	25.05	22.05	12.53	unitless	

Table II: Except for the capillary density and the number of capillaries, the parameter values in the upper part of the table, above the line, are based on experiments, while those in the lower part are derived values. The solubility and diffusivity of oxygen are constant across all compartments. Mb = myoglobin, * = estimated from our histological preparations (Fig. 2D).

ordering approximately following the typically observed order $I \leq IIa \leq IIb$.

3.4 Parameter values

The parameter values used in our model are given in Table II, based upon numerous reports in the literature (Bentley et al., 1993; Christoforides et al., 1969; Ellsworth & Pittman, 1984; Ellsworth et al., 1988; Honig & Gayeski, 1982; Jürgens et al., 1994; Mahler et al., 1985; Meng et al., 1993; Sullivan & Pittman, 1984; Goldman & Popel, 2000; Eggleton et al., 1998; Wüst et al., 2009b). The lengthscale, L , is derived by assuming that capillaries in the circular simulation domain have a dimensional density of the rat EDL muscle cross section in Fig. 2 ($\rho = 913.4 \text{ mm}^{-2}$). For convenience, the diffusivity and solubility coefficients of oxygen in interstitial spaces are assumed to equal those of muscle fibres. Although interstitial diffusivity is typically taken to be similar to that of blood *plasma*, our simulations results are insensitive to such scalings as long as the scale of interstitial spaces does not exceed a few microns. **We note here that such scales may not be valid under pathophysiological conditions and are a topic for further study (see Section 5.1 below).**

3.5 PO₂ flux lines

We seek to determine the areas of tissue where capillary PO₂ fluxes are restricted to a no-flux region surrounding each capillary, called Trapping Regions, which are generalisations of Krogh cylinders (Krogh, 1919). However, a direct way to accurately calculate oxygen supply region areas is not feasible due to the complexity of heterogeneous oxygen uptake. To proceed, we note that each such region of the muscle tissue is spanned by oxygen flux lines (or streamlines) that emerge from the enclosed capillary. We use a finite elements formulation to solve Eq. 13 for the oxygen partial pressure. The solution enables a derivation of oxygen streamlines *via*

$$\frac{dx}{ds} = -\nabla p, \quad (14)$$

and a subsequent determination of the trapping region geometries using the numerical methodologies outlined elsewhere (Al-Shammari et al., 2012).

3.6 Statistical indices

Since capillary interaction with neighbouring capillaries is excluded at the outer domain boundary by imposing a no-flux condition, we consider generating statistics for capillaries within a region of tissue where boundary artefacts are negligible, referred to as the region of interest (ROI; Egginton (1990)). The *ROI* is a square box within the disk and concentric with it, which is used to sample capillaries for statistical consideration. The edges of this region are further from the edge of the domain than the intercapillary distance and the objective is to remove domain boundary artefacts, which can be confirmed *a posteriori*. The upper and left-hand sides of the square are identified as *inclusion lines*, whilst the lower and right-hand sides are, in contrast, *exclusion lines*. A capillary domain belongs to the region of interest if it falls entirely within the box, or if it falls partly within the box and overlaps inclusion lines *only*. To ensure robust statistical measures we consider identical populations of capillaries. We emphasise that Voronoi polygons represent the capillary domains and, for definiteness, only Voronoi polygons are used to determine the inclusion criteria for the region of interest, even when the subject of study is the *trapping regions*. In addition, note that these criteria allow the tessellation of multiple regions of interest without double counting, so that it may represent the basis for considering transport processes at higher scales.

In order to quantitatively assess the correlation between Voronoi polygons and capillary supply regions, as measured by trapping regions, we use similar statistical measures to those detailed elsewhere (Al-Shammari et al., 2012). These are defined in Table III with a presentation of their numerical values for various geometries and parameter regimes given in Table IV. Additionally, we present a comparison between VP and corresponding trapping regions (TR) in terms of the LCFR index (Eqs. 2 and 4). This is shown as an average of the normalised difference of LCFR measures obtained from Voronoi polygons ($LCFR^{VP}$) and trapping regions ($LCFR^{TR}$)

$$LCFR_{\Delta} = \text{mean} \left(\frac{|LCFR_i^{TR} - LCFR_i^{VP}|}{LCFR^{TR}} \% \right). \quad (15)$$

Statistic	Symbol	Definition
Normalised mean of difference	μ_{Δ}	$\frac{\text{mean}[A(D_i)-A(V_i)]}{\text{mean}[A(D_i)]}$
Normalised standard deviation of difference	σ_{Δ}	$\frac{\text{std}[A(D_i)-A(V_i)]}{\text{mean}[A(D_i)]}$
Normalised mean of intersection	μ_{\cap}	$\frac{\text{mean}[A(D_i \cap V_i)]}{\text{mean}[A(D_i)]}$
Normalised standard deviation of intersection	σ_{\cap}	$\frac{\text{std}[A(D_i \cap V_i)]}{\text{mean}[A(D_i)]}$
Mean ratio	μ_R	$\text{mean}\left[\frac{A(V_i)}{A(D_i)}\right]$
Standard deviation of ratio	σ_R	$\text{std}\left[\frac{A(V_i)}{A(D_i)}\right]$
Normalised standard deviation of Voronoi polygons	σ_{VP}	$\frac{\text{std}[A(V_i)]}{\text{mean}[A(V_i)]}$
Normalised standard deviation of trapping regions	σ_{TR}	$\frac{\text{std}[A(D_i)]}{\text{mean}[A(D_i)]}$

Table III: Statistical measures for all capillaries i in the region of interest. D_i and V_i are the i^{th} trapping region and Voronoi polygon, respectively, and \cap denotes the spatial intersection (**overlap**) of the two domains. Here σ refers to the standard deviation, μ denotes the arithmetic mean, and $A(\cdot)$ is the non-dimensional area. See Section 4.3 for a discussion of these measures in the context of our oxygen transport simulations.

4 Results

4.1 Supply domains and histograms

4.1.1 Voronoi polygons and trapping regions

Among all random fibre type distributions for the synthetic uniform fibre size distribution, SU, the most significant perturbations of trapping region boundaries, relative to those of the Voronoi polygons, are observed in the 50:0:50 ratio of type I, IIa and IIb fibres (Fig. 4A; other distributions are not shown here). Nonetheless, for such a symmetrical fibre geometry and capillary distribution, boundaries of TR are well approximated by those of VP (Figs. 4A, C), with only slight deviations near the interface of fibres of different metabolic demands. This is not the case for increased metabolic heterogeneities (Fig. 4B), where boundary deviations of TR are much more extensive in the presence of high differential scaling of fibre-dependent O_2 uptake (e.g. 10:1 for Type I vs. Type IIb). The opposite trend, of an increasing agreement between TR and VP, is observed when the tissue is hypoxic in the presence of a non-linear O_2 consumption rate and myoglobin facilitation of intracellular O_2 diffusion (e.g. Fig. 4C).

Although the aforementioned pattern holds for all other geometries, SN (Figs. 4D-F) and H (Figs. 4G-I), boundary deviations in these cases are relatively greater in extent than those observed in the SU geometry.

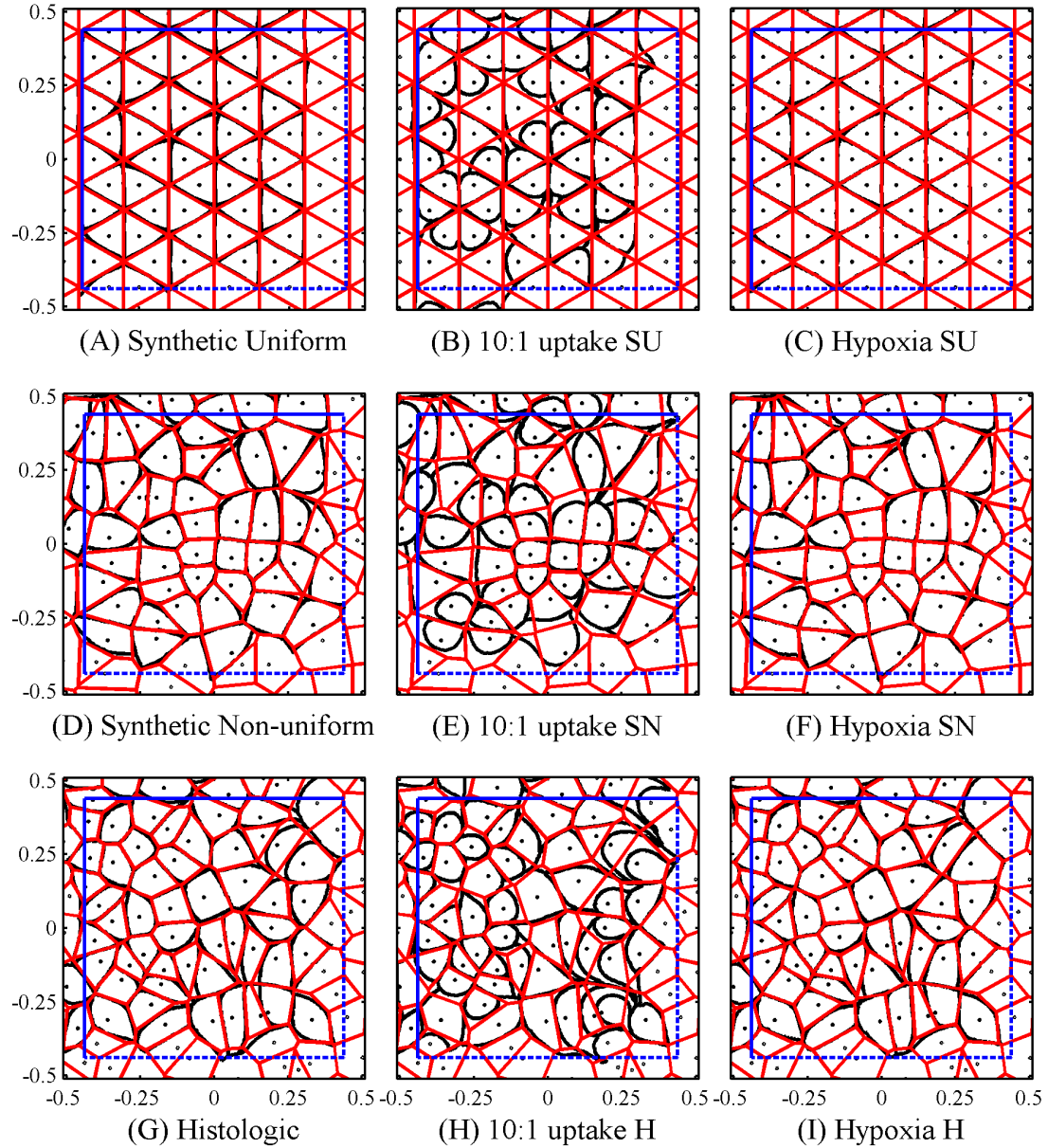


Figure 4: (A)-(I) Trapping region boundaries (black/dark) and Voronoi polygons (red/light) in the region of interest (blue/dark square: solid left/top edges and dashed right/bottom edges). There are three geometry types (Row #1 = SU with a 50:0:50 Type I to IIb proportion; Row #2 = SN with a 50:0:50 size-based Type I to IIb proportion; Row #3 = H, with fibre types assigned by size according to the observed ratio 9:37:54 for types I, IIa, and IIb, where type I fibres constitute the smallest 9%). Plots (A, D, G) represent normal conditions. Plots (B, E, H) represent a 10-to-1 Type I:Type IIb differential uptake scaling keeping the same volume-averaged tissue uptake as in (A, D, G). Tissue hypoxia ($PO_2 < 0.5 - 1$ mmHg) is simulated in plots (C, F, I) *via* increasing the oxygen uptake of all fibres by a factor of 8 (reducing capillary oxygen content gives similar results).

4.1.2 Frequency histograms

Area frequency histograms of trapping regions in the SU geometry are generally highly peaked with slightly broader distributions than Voronoi polygons (Figs. 5A, C). This is no longer the case in the presence of additional functional heterogeneities. For example, a large differential scaling in fibre-dependent uptakes for the SU case is observed to give rise to fat tails with a distinctive left-skewed distribution (Fig. 5B). Nonetheless, under hypoxic conditions such distributions are narrowed and the extended tails are less extreme (Fig. 5C).

The frequency histogram distributions for the other geometries, synthetic nonuniform (SN; Figs. 5D-F) and Histologic (H; Figs. 5G-I), are broader, partly reflecting the non-uniform distribution of fibre sizes and the asymmetry in capillary arrangements. In the SN case, the size-based fibre type arrangements with normal differential uptake (Figs. 5D, F) show TR distributions which are just as broad as those of VP, although the tails of the latter are slightly extended. Similar to SU, SN also exhibits the same left-skewed distribution when high differential scaling of uptake parameters is present (Fig. 5E), yet the tail is less extensive in this case. Moreover, the presence of hypoxic conditions shows a better histogram match with VP than the case of saturated O₂ uptake (Fig. 5D vs. Fig. 5F). These observations are also confirmed in the Histologic geometry case (Figs. 5G-I).

4.2 Qualitative observations and correlations

The behaviour of TR is described by VP with a very good agreement for all fibre distributions considered with normal ratios of differential oxygen uptake (Figs. 4A, C, D, F, G, I) though the boundaries of TR are observed to deviate slightly from Voronoi polygons as the heterogeneity in fibre size is increased.

Similarly, given normal ratios of differential oxygen uptake, the area majority of histograms of VP coincide with those of TR (Figs. 5A, C, D, F, G, I), though VP distributions are more centralised than TR when fibre size is uniform. Nonetheless, as the heterogeneity in fibre size is increased, an extended tail emerges for the VP histograms (compare Figs. 5A, D, and G), whereas histograms of trapping regions remain relatively centralised, again as long as extensive uptake heterogeneities are not present. This confirms that Voronoi polygons can both underestimate and overestimate extremes of capillary supply areas, although our observations show this effect is not extensive for non-rarefied mixed muscles with realistic fibre-size distribution.

Distributions with non-uniform fibre sizes are naturally rarefied around relatively large fibres. In particular, in the case of fibre metabolic uptake varying inversely with fibre size, glycolytic fibres are effectively rarefied. Nonetheless, the area histograms of VP are seen to essentially coincide with those of TR (Figs. 5D, F, G, I).

However, with a large differential scaling of fibre-dependent oxygen uptakes, the VP boundaries show extensive differences from trapping regions (Figs. 4B, E, H), in addition to a more pronounced deviation in shape and distribution of TR areas (Figs. 5B, E, H). The influence of such fibre-uptake scaling on distant capillaries reveals that both non-neighbouring and nearest TR expand further in the direction of more deprived fibres while, in contrast, VP are insensitive to such functional heterogeneities. Nonetheless, when the tissue is hypoxic all such

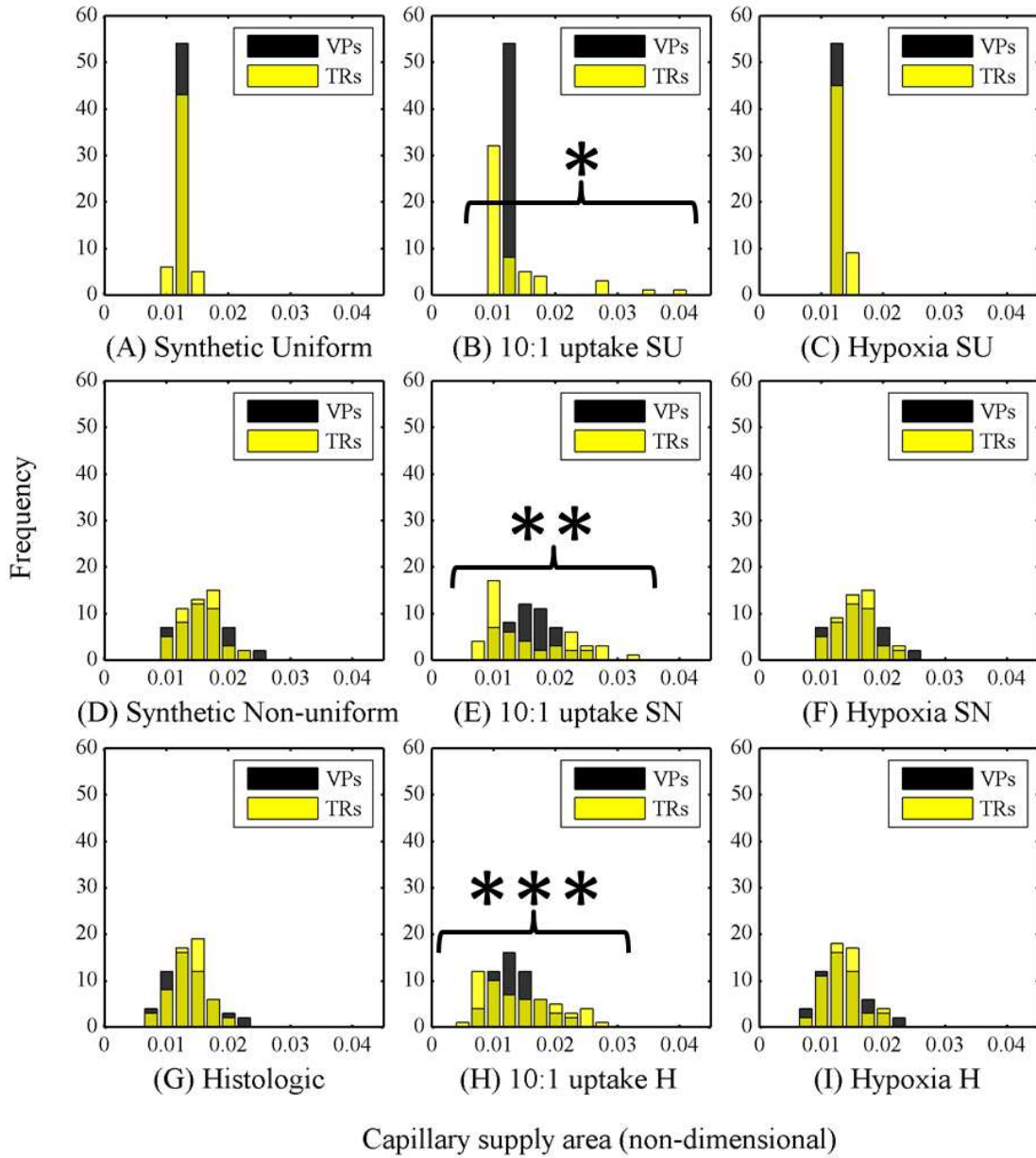


Figure 5: Frequency distributions of areas for Voronoi polygons (VP) and trapping regions (TR) within the region of interest. Histograms of the areas of Voronoi polygons are given by black/dark bars and trapping regions by light bars. Overlapping histograms are of intermediate shading. The horizontal axis represents [tissue area fractions \(supply area normalised by total tissue area\)](#) and the vertical axis shows frequency of occurrence, where the heights of the bars sum to the number of capillary domains included in region of interest. The parameters, for instance the metabolic ratios, in plots 5A-5I, are inherited from those used in Figs 4A-4I. A [two-sample Kolmogorov-Smirnov non-parametric test](#) is used to test the null hypothesis that the TR and VP samples are drawn from the same distribution. No such tests immediately applies to the SU case due to the fact that its VP distribution has a zero variance, implying that it cannot be represented by a statistical distribution with a smooth probability density. Hence, we test whether the SU cases possess a different distribution to that of the TR in plot (A). The only statistically significant failures of the null hypothesis occur for high differential uptake (plots B, E, and H). Here we have that, P , the probability the null hypothesis is satisfied, is constrained for the SU profile (*) by $P < 0.0001$, whilst for the SN (**) and H (***) cases, it is constrained by $P < 0.01$ and $P < 0.04$ respectively.

differences in area frequency distributions are reduced and the correlation between boundaries of TR and VP is improved relative to the case of abundant oxygen and thus saturating uptake.

4.3 Quantitative correlations

4.3.1 The area correlation coefficient, CC

The area correlation coefficient (CC) is a measure of the linear dependence between the VP and TR areas (and is given by their covariance divided by both of their standard deviations). Table IV demonstrates a decreased degree of correlation between the areas of VP and TR for random fibre type distributions. For such distributions, the trends in the data for random fibre types distributions is representative and shows that the highest CC is seen in the most metabolically homogenous distributions, with lowest found in the mixed oxidative-glycolytic random arrangements (50% type I, 0% type IIa, and 50% type IIb), among which the randomly rarefied SU is lowest.

Except for extremely low correlations in high differential scaling of fibre-dependent uptakes, the data also indicate that the 50:0:50 size-based distributions have generally higher CC values than all randomly mixed distributions. Moreover, the area correlation of a real mixed distribution (9% type I, 37% type IIa, and 54% type IIb) is found to be greater than that of the 50:0:50 size-based cases, with hypoxia being the only exception where CC is found to be highest across all mixed fibre-type distributions. Additional simulations (not shown) show similar trends for the EDL muscle fibre distribution (H), although higher corresponding values are observed in this case.

4.3.2 The means μ_{Δ} , μ_{\cap} , μ_R , $LCFR_{\Delta}$

The *normalized mean of difference* (μ_{Δ}) provides a measure for the degree of failure of Voronoi polygons to cover comparable areas to those of trapping regions. This is observed to correlate with heterogeneities in fibre functional characteristics, fibre size, and capillary distributions.

For symmetrical capillary and fibre distributions (SU), this statistic increases with increased heterogeneity in fibre type composition with the 50:0:50 proportion of types I, IIa, IIb being the highest ($\mu_{\Delta} = 0.0679$). However, introducing fibre type IIa (9:37:54) leads to a slightly smaller value ($\mu_{\Delta} = 0.0473$). Further functional heterogeneities, such as down-scaling the oxygen uptake of type IIb fibres by a factor of 5, lead to a 332% increase in μ_{Δ} value ($\mu_{\Delta} = 0.3008$ vs. 0.0697). In contrast, a 10% random capillary rarefaction leads to a 78.6% increase in μ_{Δ} value ($\mu_{\Delta} = 0.1245$ vs. 0.0697), and a 50% reduction in capillary density increases μ_{Δ} by only 7.5% ($\mu_{\Delta} = 0.0749$ vs. 0.0697). However, when tissue PO_2 falls below 0.5-1 mHg (hypoxia) the areas covered by VP are generally improved by 35.6% with respect to areas of TR ($\mu_{\Delta} = 0.0449$ vs. 0.0697).

With fibre size heterogeneities introduced in the SN geometry, a comparison with the homogeneous fibre-type distribution in the SU geometry shows a marked increase in μ_{Δ} ($\mu_{\Delta} = 0.1209$ vs. 0.0077 in the 100:0:0 composition). As these two cases are of a similar non-mixed metabolic character (i.e. uniform fibre type), it is clear that such a deviation in mean normalised difference is a direct result of the heterogeneity in capillary spacing inherent in the

		μ_{Δ}	σ_{Δ}	μ_{\cap}	σ_{\cap}	μ_R	σ_{VP}	σ_{TR}	CC	$LCFR_{\Delta}$	
Random	0:0:100	SU	0.0072	0.0073	0.9845	0.0028	0.9941	0	0.0073	*	0.19
		SN	0.1206	0.1455	0.8951	0.1800	1.0005	0.2528	0.1274	0.9307	6.44
	25:0:75	SU	0.0245	0.0291	0.9605	0.0339	1.0094	0	0.0301	*	3.46
		SN	0.1416	0.1794	0.8705	0.1697	1.0119	0.2528	0.1445	0.7381	9.05
	50:0:50	SU	0.0697	0.0882	0.9255	0.0382	1.0001	0	0.0882	*	4.60
		SU _R	0.1245	0.1612	0.8788	0.1065	1.0007	0.1983	0.1012	0.5901	7.41
		SN	0.1600	0.1955	0.8701	0.1671	1.0228	0.2528	0.1359	0.6770	8.18
	75:0:25	SU	0.0239	0.0285	0.9617	0.0329	1.0103	0	0.0285	*	3.10
		SN	0.1380	0.1680	0.8850	0.1763	1.0084	0.2528	0.1637	0.7662	6.93
	100:0:0	SU	0.0077	0.0078	0.9844	0.0030	0.9940	0	0.0078	*	0.23
		SN	0.1209	0.1448	0.8955	0.1805	1.0011	0.2528	0.1274	0.9340	6.43
	Size based	SN	0.1115	0.1381	0.9084	0.1961	1.0103	0.2528	0.1886	0.8508	4.97
	Real	SU	0.0473	0.0599	0.9447	0.0306	1.0042	0	0.0606	*	3.80
		SN	0.1048	0.1284	0.9114	0.1933	1.0025	0.2528	0.1757	0.8875	4.64
		H	0.1129	0.1451	0.8842	0.2136	0.9728	0.2854	0.1996	0.8692	3.41
	Low CD	SU	0.0749	0.0931	0.9182	0.0408	1.0000	0	0.0931	*	4.93
		SN	0.1150	0.1422	0.9065	0.1959	1.0098	0.2528	0.1894	0.8380	4.89
		H	0.1186	0.1530	0.8782	0.2104	0.9710	0.2854	0.1972	0.8485	3.72
Uptake scale	SU	0.3008	0.4803	0.7615	0.0990	1.0833	0	0.4803	*	24.27	
	SN	0.3122	0.3742	0.7700	0.2257	1.1529	0.2528	0.4362	0.5195	19.25	
	H	0.2633	0.3118	0.7509	0.2626	1.0386	0.2854	0.4208	0.6723	17.95	
MM+Mb	SU	0.0689	0.0862	0.9244	0.0383	1.0004	0	0.0862	*	4.47	
	SN	0.1113	0.1374	0.9088	0.1968	1.0085	0.2528	0.1900	0.8510	4.96	
	H	0.1128	0.1454	0.8839	0.2134	0.9723	0.2854	0.1997	0.8681	3.46	
Hypoxia	SU	0.0449	0.0551	0.9507	0.0244	0.9967	0	0.0551	*	2.96	
	SN	0.0916	0.1128	0.9237	0.2058	1.0037	0.2528	0.1959	0.9082	3.83	
	H	0.0894	0.1143	0.9112	0.2334	0.9793	0.2854	0.2132	0.9312	2.19	

Table IV: Statistics determined from areas of Voronoi polygons and trapping regions for the Synthetic Uniform (SU), Synthetic Non-uniform (SN) and Histologic (H) geometries under different fibre type/size distributions and parameter regimes. A list of ratios (e.g. 25:0:75) denotes the fibre type proportion distribution I:IIa:IIb (composition) for the row, with a distribution 9:37:54 for the image-based *real* case of rat EDL muscle. In the case of *size-based* fibre type distribution of the SN geometry, a 50:0:50 ratio is used. Distinct parameter regime entries are denoted by *Low CD* (a 50% reduction in capillary density), *Uptake scale* (a fibre-type dependent oxygen demand scaling of 1:0.88:0.1), *MM+Mb* (Michaelis-Menten kinetics & myoglobin-facilitated diffusion), and *Hypoxia* (for MM+Mb together with the presence of hypoxic tissue regions, $PO_2 < 0.5$ -1 mmHg). Hypoxia is achieved by increasing fibre uptake by a factor of 8. Unless otherwise specified, the entries for each row correspond to a random 50:0:50 fibre type distribution for the SU geometry, a size-based 50:0:50 fibre type distribution for the SN geometry, and a real 9:37:54 fibre-type distribution of for the H geometry. Entries denoted by * denote cases where statistics are not applicable. The area correlation coefficient, CC , is ill-defined for hexagonal arrays since all areas are the same, and hence their standard deviation is null. Nonetheless, it is clear that Voronoi polygon areas provide exceedingly good estimates of trapping region areas in this case. Note that the value of σ_{TR} under perfect symmetry reflects the scale of the boundary artefacts. See Eq. 15 for a definition of $LCFR_{\Delta}$.

SN geometry rather than a consequence of functional fibre heterogeneities, which are absent in this case. This implies that statistical values generated for a tissue with a uniform metabolic demand may serve as a baseline for exploring the functional effects of capillary asymmetries. For example, increasing the proportion of mixed fibre types influences μ_Δ less for distributions with non-uniform fibre size ($\mu_\Delta = 0.1600$ vs. 0.1206) than distributions with uniform fibre size ($\mu_\Delta = 0.0697$ vs. 0.0072), **even in absolute terms**.

Fibre size heterogeneities are also present in the H (histologic) geometry where, additionally, interstitial spaces add more to the spatial heterogeneity of capillaries. Given an EDL fibre-type composition (9:37:54), the H geometry shows higher μ_Δ values than those of the size-based SN and SU ($\mu_\Delta = 0.1129$ vs. 0.1048 and 0.0473 , respectively). This likely reflects the heterogeneity in capillary spacing, which is highest in the H geometry (σ_{VP} is a measure of capillary heterogeneity). In contrast, despite the observation that high differential scaling of oxygen uptake increases μ_Δ for all geometries, we note that the Histologic case has the lowest μ_Δ value ($\mu_\Delta = 0.2633$ vs. 0.3122 for SN and 0.3008 for SU). Noting that the effect of high differential uptake is expected to be more pronounced at the interface of dissimilar fibre types, the above change in μ_Δ trend is likely due the smaller interface in the Histologic geometry which is reflected in the aggregation of similar fibre types.

The *normalized mean of intersection* (μ_\cap) and the *mean ratio* (μ_R) describe how well Voronoi polygons capture the functional capillary supply of trapping regions, with values of unity for cases of a perfect match. Mean ratio values further infer whether, on average, a VP is over- ($\mu_R > 1$) or underestimating ($\mu_R < 1$) the functional capillary supply.

The value of μ_\cap decreases with increased proportion of fibre types in SN and SU for random fibre type distributions, with SU distributions showing relatively higher values than SN. However, the decay of μ_\cap with respect to the proportion of mixed fibres is less in SN than SU. In addition, fibre distributions where a size-type correlation is enforced (size of Type I < Type IIa < Type IIb) show markedly higher μ_\cap values than randomly distributed fibre types of random size allocation ($\mu_\cap = 0.908$ vs. 0.87). In contrast, such values are significantly lower when differential scaling of fibre demand is present (e.g. $\mu_\cap = 0.77$ for SN). In addition, under the same conditions, an overestimate of functional capillary supply is evident (e.g. $\mu_R = 1.1529$ for SN). Conversely, when the tissue is hypoxic, there is a general improvement in the overlap of a Voronoi polygon with the corresponding trapping region ($\mu_\cap = 0.9084$ vs. 0.9237 for the SN 50:0:50 size-based distribution; $\mu_\cap = 0.9255$ vs. 0.9507 for the SU 50:0:50 distribution; $\mu_\cap = 0.8842$ vs. 0.9112 for the H distribution of EDL muscle).

Given that LCFR represents the number of capillary supply equivalents at maximum capacity, the mean of normalised difference of the LCFR indices, $LCFR_\Delta$, provides a measure of the degree of failure of VP-based capillary supply indices. As expected in the case of perfect capillary symmetry (SU) and uniform tissue uptake (100% Type I or Type IIb), this index is very small ($< 0.25\%$). However, even for this geometry, a random increase in the heterogeneity of fibre-type composition leads to a **marked** increase in $LCFR_\Delta$ value ($LCFR_\Delta = 0.23$ vs. 4.6). Similarly, the same trend is observed in the case of non-uniform fibre-size distribution, although the increase in $LCFR_\Delta$ is **notably less** ($LCFR_\Delta = 6.43$ vs. 8.18). Moreover, under normal differential **uptake**, the highest values of $LCFR_\Delta$ correspond to tissues with fibres of highly mixed types and random size (SU = 3.1-4.6% and SN = 6.93-9.05%). Conversely, the case of size-based fibre-type distributions shows a significant decrease in $LCFR_\Delta$, with lowest values observed in hypoxic tissues where oxygen consumption is adjusted significantly below maximum oxygen consumption ($MO_{2,max}$). It is interesting to note here that the SN geometry

with a size-based fibre type distribution has a smaller value of $LCFR_{\Delta}$ than the rarefied SU geometry whose underlying capillary distribution is more symmetrical ($LCFR_{\Delta} = 4.97$ for SN vs. 7.41 for SU).

In all cases, introducing an extreme uptake heterogeneity, such as a high differential fibre O_2 uptake, leads to the highest discrepancy between VP-based and TR-based LCFR, **where values are largest for the SU case and smallest for the histological case.**

4.3.3 The normalized standard deviations σ_{Δ} , σ_{\cap} , σ_{VP} , σ_{TR}

The normalised standard deviations increase with greater heterogeneity in fibre-type composition and size distribution. The highest values correspond to the greatest degree of functional heterogeneity, i.e. high differential scaling of different fibre type-specific O_2 uptake.

The *normalized standard deviation of difference* (σ_{Δ}) describes the difference between the spread of Voronoi polygon areas and that of trapping regions. This measure is found to follow the same trends as those of μ_{Δ} illustrating that the spread of VP areas begins to differ from that of TR for increased mixing of fibre types. In particular, random mixing of fibre types shows higher values of σ_{Δ} than size-based and real distributions.

The *normalized standard deviation of intersection* σ_{\cap} extends the above correlations by considering the spread of VP areas that overlap with TR. This statistic tends monotonically toward the value of σ_{VP} as the oxygen demand and the capillary arrangement become increasingly homogeneous. Here σ_{VP} quantifies the asymmetry in the underlying capillary distribution, with increasing values corresponding to greater asymmetries. Also, the presence of size-based fibre-type distributions further shifts σ_{\cap} in the direction of σ_{VP} , with hypoxic conditions showing the largest shift. This illustrates that the spread of the VP-TR overlap is reduced as the Voronoi polygons areas conform more to those of trapping regions when fibre type distributions are less random.

The dispersion in oxygenation supply areas, as measured by σ_{VP} and σ_{TR} , remains essentially zero for the SU geometry with uniform fibre-type composition ($\sigma_{VP} = 0$, $\sigma_{TR} = 0.0073$, where the value of σ_{TR} under perfect symmetry reflects the scale of the boundary artefacts). However, both spread statistics begin to widen as structural and functional heterogeneities are increased. In particular, despite the fact that there is no dispersion in VP areas in the SU geometry, the spread in TR areas is found to be increasingly positive across all mixed fibre composition. In the SN geometry, however, the spread in TR areas is generally smaller than that of VP areas, except for the case of an extreme functional heterogeneity (high differential uptake). These observations indicate that TR are influenced by functional changes in the diffusive and metabolic properties, whereas VP are not, highlighting an advantage of trapping regions.

5 Discussion & conclusions

Techniques for the assessment of muscle capillary supply vary widely within the literature. Global methods are often used to analyse capillarisation where average values of structural composition or functional activity are taken to represent the whole tissue uniformly. However,

such measures cannot capture the spatial heterogeneity in capillary supply generated by the local metabolic environment and variations in fibre size. In addition, the scale-dependency inherent in such indices may explain why data on capillarity is variable, if not conflicting (Egginton, 1990). On the other hand, the space-filling area-based method of capillary domains is used to avoid the spatial limitations of analyses based on global indices. In particular, space-filling methods have the advantage of capturing the local environment of capillaries by giving each a 2-dimensional domain representing its maximal supply area, and therefore take into account heterogeneities in oxygen supply and demand, while also allowing exploration of local influences of microvascular remodelling and regulation. In addition, the validity of using capillary domains (Voronoi polygons) to represent capillary supply areas has been recently confirmed for general cases of muscle tissue with uniform oxygen uptake (Al-Shammari et al., 2012). Whether this **representation** is sufficiently accurate to describe functionally heterogeneous tissues is not clear. Hence, our present study considered when capillary domains are appropriate to assess O₂ supply from capillary distributions embedded in functionally heterogeneous muscle tissues, e.g. skeletal muscle, by exploring their correlation with a biophysically based alternative, namely the trapping regions.

Voronoi polygons (VP) and trapping regions (TR) are observed to have the same qualitative shapes and overall quantitative distributions for all fibre distributions in a maximally perfused, non-rarefied, metabolically heterogeneous system regardless of the degree of structural asymmetry even for hypoxic tissues. This correlation is lowest in muscle with a highly heterogeneous fibre type composition, assuming the other conditions above are met. However, even in this case the normalised mean of the VP areas overlapping TR remains above 87%, provided that noticeable capillary rarefactions or significant heterogeneities in fibre-dependent O₂ uptake are absent. This remains true across all synthetic capillary and fibre distributions (type & size), and for those extracted from an EDL muscle tissue cross section. These observations are also robust to variations in the adjustable parameters of the transport model (Al-Shammari et al., 2012). Therefore, in the absence of extremes that are only associated with pathologies, our modelling predicts that VP provide a computationally simple and accurate approximation of functional capillary supply for muscle tissue cross sections of heterogeneous fibre types, which in turn theoretically validates the conclusions of modelling studies taking Voronoi polygons as a basis for morphometric analyses of maximal capillary supply in skeletal muscle tissues (Degens et al., 1992, 2002, 2006, 2008; Egginton et al., 2001; Wüst et al., 2009a; Ahmed et al., 1997).

A local increase in fibre area (local hypertrophy) lowers the accuracy of VP as it effectively leads to local capillary rarefaction, which is consistent with our recent predictions for homogeneous muscle tissue (Al-Shammari et al., 2012) and also the numerical observations that fibre size influences PO₂ heterogeneity (Liu et al., 2012). However, if such hypertrophies are localised to fibres with relatively low O₂ uptake (i.e. glycolytic fibres), a balance resulting between opposing PO₂ fluxes is observed as indicated for instance by the increase in μ_{\cap} and decrease in μ_{Δ} for size-based fibre type distribution. The overall accuracy of VP within the region of interest may then only change slightly, thus potentially retaining their validity in representing capillary supply areas. These observations suggest that the lower anatomical capillary supply to glycolytic fibres *in situ* is balanced by their reduced oxygen demand per unit volume. In turn, the high VP-TR correlation for rat EDL tissue perhaps suggests that the fibre type distribution may be tightly regulated to avoid large fibres with high oxidative capacities per fibre volume. Similarly, our findings also suggest that a local homogeneity in capillary supply is necessary when the specific oxygen demand of nearby fibres is relatively high, **in agreement**

with the findings of Egginton et al. (1988).

The loss of capillaries *via* random capillary rarefactions, regardless of the local metabolic character, significantly decreases the correlation between VP and TR. In contrast, a global rarefaction *via* a reduction in mean capillary density only slightly perturbs the VP-TR correlation. A global reduction in capillary density increases diffusion distances and is effectively equivalent to an increase in the non-dimensionalised oxygen uptake of the biophysical model. Nonetheless, the effect of such increase in non-dimensional MO_2 on the VP-TR correlation is relatively small compared to that of random local rarefactions, and can be simply balanced by a parallel global decrease in oxygen consumption. This highlights the robustness of the estimates for the capillary supply regions for such parameter changes and entails that the correlation between VP and TR is only weakly affected by global changes, in comparison to the influence of local rarefactions.

A common assumption is that the oxidative capacity or functional characteristics of different muscles depends on fibre type composition (i.e. proportion of Type I, IIa, and IIb). However, a random arrangement of fibre types may lead to significantly weaker correlations between VP and TR. This observation shows that, in addition to fibre type composition, oxidative capacity depends on the distribution of fibre types, in a close parallel with the relationship between functional capillary density and capillary distribution. Hence, the modelling observations are consistent with the hypothesis that to avoid heterogeneities in oxygen supply fibre type distribution may need to be tightly regulated to avoid large fibres with high oxidative capacities per fibre volume. This, in turn, maximises the benefit from the smallest number of capillaries, thus minimising costs of maintenance.

Increasing the degree of differential oxygen uptake, the ratio of oxidative to glycolytic MO_2 , has a significant impact on the accuracy of VP relative to TR for all tissue geometries. This effect is on the scale of a severe local rarefaction (Al-Shammari et al., 2012) and is expected to be far greater than the heterogeneities resulting from local fibre hypertrophies. This indicates that VP may be of limited use and inaccurate in assessing capillary supply areas for physiological situations associated with high degree of fibre differential uptake (Nakatani et al., 1999), such as altered patterns of fibre recruitment (Gregory & Bickel, 2005), and perhaps during muscle remodelling such as an increase in mitochondrial volume densities (Wüst et al., 2012). However, aggregation of similar fibres as observed in histological cross sections mitigates the impact of a high differential uptake on the accuracy of VP. In particular, grouping of the same fibre type in clusters provides a region of uniform uptake that is large enough to prevent PO_2 fluxes of interior capillaries from reaching remote fibres with high demands, thus acting as a local buffer to restrict capillary supply areas from remote supply. Capillaries near the periphery of a fibre cluster, however, are exposed to the oxidative-glycolytic interface and thus the direction of their O_2 fluxes will be forced into the oxidative side resulting in complex flux lines that cannot be accommodated within the pure geometrical construct of VP. Nonetheless, the overall effect has a low impact on the quality of VP in capturing capillary supply regions. The high correlations between VP and TR in rat EDL muscle therefore also suggest that the anatomical fibre distribution is also tightly regulated to prevent large surface area of interaction between metabolically dissimilar fibres.

Surprisingly, under conditions leading to tissue hypoxia VP appear to approximate oxygen supply regions to a better extent than under normal conditions. Indeed, under conditions of low oxygenation, myoglobin facilitated transport is additionally considered and the muscle tissue consumption is adjusted to very low values in accordance with Michaelis-Menten kinet-

ics, thus decreasing PO_2 fluxes from remote capillaries and between fibres. Due to the PO_2 dependence of the Michaelis-Menten curve under such conditions, the local oxygen uptake of dissimilar fibres will become much more homogeneous, which in turn leads to substantial reduction in the extent of oxygen differential uptake. In addition, given that a VP distribution reflects the underlying distribution of capillaries, the observation that predictions of oxygen supply areas (TR) approach those of VP suggests that in chronically hypoxic tissues capillary distribution is more important than fibre demand for oxygen.

The current data and modelling demonstrate that VP and TR tend to coincide with reasonable accuracy for a capillary bed dispersed in a mixed fibre population without high differential uptake, indicating that each region within such tissue is supplied by its nearest capillary. This in turn suggests a lack of redundant capillaries within such tissue, which is found in almost all human skeletal muscles. In other mammals, however, regional specialisations in function have led to clustering of more oxidative or more glycolytic populations of fibres. For example, in the rat *tibialis anterior* (TA) the outer cortex is almost all Type IIB fibres, whereas the inner core is a mix of Type I and Type IIA fibres, while the *soleus* is nearly all Type IIA fibres. Our data indicate that VP and TR are expected to coincide with higher degree of accuracy in the outer cortex of rat TA and Soleus muscles than in the inner core of the TA muscle due to the **latter's** more abundant interfacial regions of dissimilar fibre types. This highlights that efficient capillary supply during the development of such muscles need not always be dominantly constrained to oxygen delivery, especially in the presence of relatively high differential uptake between fibre types as can occur during fibre remodelling (Wüst et al., 2012). **In particular, since the VP and TR deviate in such muscle, not every capillary is simply supplying oxygen to the tissue closest to it. Hence, in this context there is supply inefficiency in that, in various locations, the structure of the tissue entails that distant capillaries compensate nearby capillaries, so that the latter are not fully utilised. This, in turn, suggests that the control of capillary distribution in mixed muscles can also be affected by other feedback regulators in addition to oxygen and also muscle fibre type distribution and composition.**

5.1 Model extensions and limitations

For convenience, the compartment-dependent diffusive parameters (solubility and diffusivity) of our model were assumed to be uniform in our simulations, although actual values may not be. Parallel simulations based on non-uniform diffusive parameters have shown a general improvement in the correlation between Voronoi polygons and trapping regions, although not significant enough to alter any of the trends observed in our current results. Further, the current model geometries are limited in terms of intra-fibre resolution, but it can be extended to investigate finer micro-architecture resolution such as the non-uniform mitochondrial distributions observed in oxidative fibres *via* aggregations under **the** fibre *sarcolemma* (Martin & Edgerton, 1992; Hoofd & Egginton, 1997). This can be modelled by allowing for intracellular uptake compartmentalisation whereby an oxidative fibre is composed of two metabolically distinct zones: a sub-sarcolemmal zone of higher uptake per unit volume and an inter-myofibrillar region of lower uptake. Other feasible extensions could be concerned with the cases of *oedema* and *fibrosis*, where the interstitial parameters and scale become important **and also the influence of arterioles and venules on oxygen supply regions, rather than focussing on regions of tissue where larger vessels are not present.** Finally, since our model predicts the behaviour of this system in the context of maximal capillary supply capacity where intravascular convection and

intercellular axial diffusion are neglected, our results are currently restricted to 2-dimensional muscle cross sections, but are in principle extendable to 3-dimensional image stacks. **In particular, our model can be extended to allow for sub-maximal capillary supply under conditions of sub-maximal oxygen uptake and increased perfusion heterogeneities as well as geometrical details such as capillary cross bridges and tortuous or oblique capillaries.**

5.2 Summary

While the Voronoi polygon approximation to trapping regions depends on heterogeneity of fibre composition, it is nonetheless representative for maximal vascular capacity given the absence of **capillary** rarefaction and high differential uptake **between fibres**, while also exhibiting insensitivity to model parameters. Therefore, measures of muscle capillary supply capacity based on Voronoi polygons may be reasonably used for mixed muscle samples. However, increases in heterogeneity associated differential uptake will eventually lower the accuracy of Voronoi polygons. Hence, more sophisticated measures of capillary supply capacity should be used to study structural or functional dysregulation in striated muscle tissues, when flux trapping regions may provide a more robust representation of capillary supply regions. In addition, the relationships between Voronoi polygons and trapping regions may be generally informative in studies exploring the regulatory mechanisms underlying the capillary and fibre distributions in skeletal muscles.

6 Disclosures

No conflict of interest, financial or otherwise, are declared by the authors.

7 Author Contributions

AAA, EAG, and SE conceived and designed the experiments. SE contributed muscle samples, staining reagents, and tissue preparation materials and tools. AAA performed numerical experiments, analysed data, contributed analysis tools, and prepared figures. AAA, EAG, and SE interpreted the results, drafted the manuscript, edited and the revised the manuscript, and approved the final version of the manuscript.

8 Acknowledgement

The authors would like to thank Alan Benson for useful feedback at an earlier stage of the manuscript, and the anonymous referees for their valuable comments. The first author also wishes to acknowledge the generous support through a graduate scholarship from Kuwait University, Kuwait.

References

- Ahmed SK, Egginton S, Jakeman PM, Mannion AF, & Ross HF. Is human skeletal muscle capillary supply modelled according to fibre size or fibre type? *Experimental Physiology*, 1997;82(1):231-234.
- Al-Shammari AA, Gaffney EA, & Egginton S. Re-evaluating the use of Voronoi Tessellations in the assessment of oxygen supply from capillaries in muscle. *Bulletin of Mathematical Biology*, 2012;74(9):2204-31.
- Badr I, Brown M, Egginton S, Hudlická O, Milkiewicz M, & Verhaeg J. Differences in local environment determine the site of physiological angiogenesis in rat skeletal muscle. *Experimental Physiology*, 2003;88(5):565-568.
- Martin TP, & Edgerton VR. Intrafibre distribution of succinate dehydrogenase in cat tibialis anterior motor units. *Canadian Journal of Physiology and Pharmacology*, 1992;70:970-976.
- Bentley TB, Meng H, & Pittman RN. Temperature-dependence of oxygen diffusion and consumption in mammalian striated-muscle. *Am J Physiol*, 1993;264(6):H1825-H1830.
- Christoforides C, Laasberg LH, & Hedley-Whyte J. Effect of temperature on solubility of O₂ in human plasma. *J Appl Physiol*, 1969;26:56-60.
- Degens H, Turek Z, Hoofd LJC, Vanthof MA, & Binkhorst RA. The relationship between capillarization and fiber types during compensatory hypertrophy of the plantaris muscle in the rat. *Journal Of Anatomy*, 1992;180(Part 3):455-463.
- Degens H, Anderson RK, & Alway SE. Capillarization in skeletal muscle of rats with cardiac hypertrophy. *Medicine and Science in Sports and Exercise*, 2002;34(2):258-266.
- Degens H, Deveci D, Botto-Van Bemden A, Hoofd LJC, & Egginton S. Maintenance of heterogeneity of capillary spacing is essential for adequate oxygenation in the soleus muscle of the growing rat. *Microcirculation*, 2006;13(6):467-476.
- Degens H, Kosar SN, Hopman MTE, & de Haan A. The time course of denervation-induced changes is similar in soleus muscles of adult and old rats. *Applied Physiology Nutrition and Metabolism*, 2008;33(2):299-308.
- Deveci D, & Egginton S. Muscle ischaemia in rats may be relieved by overload-induced angiogenesis. *Experimental Physiology*, 2002;87(4):479-488.
- Ebina T, Hoshi N, Kobayashi M, Kawamura K, Nanjo H, Sugita A, et al., Physiological angiogenesis in electrically stimulated skeletal muscle in rabbits: characterization of capillary sprouting by ultrastructural 3-D reconstruction study. *Pathology International*, 2002;52(11):702-712.
- Egginton S, Turek Z, & Hoofd LJC. Differing patterns of capillary distribution in fish and mammalian skeletal muscle. *Respiration Physiology*, 1988;74(3):383-396.
- Egginton S, & Ross HF. Quantifying capillary distribution in four dimensions. *Advances in Experimental Medicine and Biology*, 1989;248:271-280.

- Egginton S. Numerical and areal density estimates of fiber type composition in a skeletal muscle (rat extensor digitorum longus). *Journal of Anatomy*, 1990;168:73-80.
- Egginton S, & Ross HF. In: Planar analysis of tissue capillary supply. Society for Experimental Biology Seminar Series 51: Oxygen Transport in Biological Systems. Cambridge University Press, 1992:pp. 165-195.
- Egginton S, Fairney J, & Bratcher J. Differential effects of cold exposure on muscle fibre composition and capillary supply in hibernator and non-hibernator rodents. *Experimental Physiology*, 2001;86(5):629-639.
- Egginton S. Temperature and angiogenesis: the possible role of mechanical factors in capillary growth. *Comparative Biochemistry and Physiology Part A, Molecular and integrative physiology*, 2002;132(4):773-787.
- Egginton S, & Gaffney EA. Tissue capillary supply-it's quality not quantity that counts! *Experimental Physiology*, 2010;95(10):971-979.
- Eggleton CD, Roy TK, & Popel AS. Predictions of capillary oxygen transport in presence of fluoro-carbon additives. *American Journal of Physiology*, 1998;275:H2250-H2257.
- Eggleton CD, Vadapalli A, Roy TK, & Popel AS. Calculations of intracapillary oxygen tension distributions in muscle. *Mathematical Biosciences*, 2000;167:123-143.
- Ellsworth ML, Popel AS, & Pittman RN. Assessment and impact of heterogeneities of convective oxygen transport parameters in capillaries of striated muscle: experimental and theoretical. *Microvascular Research*, 1988;35:341-362.
- Ellsworth ML, & Pittman RN. Heterogeneity of oxygen diffusion through hamster striated muscles. *Am J Physiol*, 1984;246:H161-H167.
- Fletcher JE. On facilitated oxygen diffusion in muscle tissue. *Biophysical Journal*, 1980;29:437-458.
- Gayeski TEJ, & Honig CR. Intracellular PO₂ in long axis of individual fibers in working dog gracilis muscle. *American Journal of Physiology*, 1988;254:H1179-H1186.
- Goldman D. Theoretical models of microvascular oxygen transport to tissue. *Microcirculation*, 2008;15(8):795-811.
- Goldman D, & Popel AS. A computational study of the effect of capillary network anastomoses and tortuosity on oxygen transport. *Journal of Theoretical Biology*, 2000;206:181-194.
- Gregory CM, Bickel CS. Recruitment patterns in human skeletal muscle during electrical stimulation. *Physical Therapy*, 2005;85(4):358-64.
- Hoofd L, Turek Z, Kubat K, Ringnalda BEM, & Kazda S. Variability of intercapillary distance estimated on histological sections of rat heart. In: Oxygen Transport to Tissue-VII. Eds. Kreuzer F, Cain SM, Turek Z, & Goldstick TK, Plenum Press, New York, 1985;pp. 239-247.
- Hoofd L, Olders J, & Turek Z. Oxygen pressures calculated in a tissue volume with parallel capillaries. *Advances in Experimental Medicine and Biology*, 1990;277:21-9.

- Hoofd L, & Egginton S. The possible role of intracellular lipid in determining oxygen delivery to fish skeletal muscle. *Respiration Physiology*, 1997;107:191-202.
- Honig CR, & Gayeski TE. Correlation of O₂ transport on the micro and macro scale. *Int J Microcirc Clin Exp*, 1982;1:367-380.
- Hudlická O, Brown M, & Egginton S. Angiogenesis in skeletal and cardiac muscle. *Physiological Reviews*. 1992;72(2):369-417.
- Jürgens KD, Peters T, & Gros G. Diffusivity of myoglobin in intact skeletal muscle cells. *Proceedings of the National Academy of Sciences of the United States of America*, 1994;91(9):3829-3833.
- Krogh A. The number and distribution of capillaries in muscles with calculations of the oxygen pressure head necessary for supplying the tissue. *The Journal of Physiology*, 1919;52(6):409-415.
- Liu G, Mac Gabhann F, & Popel AS. Effects of fiber type and size on the heterogeneity of oxygen distribution in exercising skeletal muscle. *PLoS ONE*, 2012;7:e44375.
- Mahler M, Louy C, Homsher E, & Peskoff A. Reappraisal of diffusion, solubility, and consumption of oxygen in frog skeletal muscle, with applications to muscle energy balance. *The Journal of General Physiology*, 1985;86(1):105-134.
- Meng H, Bentley TB, & Pittman RN. Myoglobin content of hamster skeletal muscles. *Journal of Applied Physiology*, 1993;74(5):2194-2197.
- Nakatani T, Nakashima T, Kita T, Hirofuji C, Itoh K, Itoh M, and Ishihara A. Succinate dehydrogenase activities of fibers in the rat extensor digitorum longus, soleus, and cardiac muscles. *Archive of Histology and Cytology*, 1999;62(4):393-399.
- Scott GR, Egginton S, Richards JG, & Milsom WK. Evolution of muscle phenotype for extreme high altitude flight in the bar-headed goose. *Proceedings of the Royal Society B*, 2009;276(1673):3645-3653.
- Sullivan SM, & Pittman RN. In vitro O₂ uptake and histochemical fiber type of resting hamster muscles. *Journal of Applied Physiology Respiratory Environmental and Exercise Physiology*, 1984;57(1):246-253.
- Suzuki J, Kobayashi T, Uruma T, & Koyama T. Strength training with partial ischaemia stimulates microvascular remodelling in rat calf muscles. *European Journal of Applied Physiology*, 2000;82(3):215-222.
- Wang CY, & Bassingthwaite JB. Capillary supply regions. *Mathematical Biosciences*, 2001;173(2):103-114.
- Whiteley JP, Gavaghan DJ, & Hahn CE. Mathematical modelling of oxygen transport to tissue. *Journal of Mathematical Biology*, 2002;44(6):503-522.
- Wüst RCI, Jaspers RT, van Heijst AF, Hopman MTE, Hoofd LJC, van der Laarse WJ, & Degens H. Region-specific adaptations in determinants of rat skeletal muscle oxygenation to chronic hypoxia. *American Journal of Physiology*, 2009;297(1):H364-H374.

Wüst RCI, Gibbings SL, & Degens H. Fiber capillary supply related to fiber size and oxidative capacity in human and rat skeletal muscle. In: Liss P, Hansell P, Bruley DF, & Harrison DK, Eds. *Oxygen Transport to Tissue XXX*. vol. 645 of *Advances in Experimental Medicine and Biology*, 2009:pp. 75-80.

Wüst RCI, Myers DS, Stones R, Benoist D, Robinson PA, Boyle JP, Peers C, White E, & Rossiter HB. Regional skeletal muscle remodeling and mitochondrial dysfunction in right ventricular heart failure. *American Journal of Physiology, Heart Circulatory Physiology*, 2012;302(2):H402-H411.